

Berry curvature dipole in Weyl semimetal materials: An *ab initio* studyYang Zhang,^{1,2} Yan Sun,¹ and Binghai Yan^{3,*}¹Max Planck Institute for Chemical Physics of Solids, 01187 Dresden, Germany²Leibniz Institute for Solid State and Materials Research, IFW Dresden, 01069 Dresden, Germany³Department of Condensed Matter Physics, Weizmann Institute of Science, Rehovot 7610001, Israel

(Received 29 August 2017; published 3 January 2018)

Noncentrosymmetric metals are anticipated to exhibit a dc photocurrent in the nonlinear optical response caused by the Berry curvature dipole in momentum space. Weyl semimetals (WSMs) are expected to be excellent candidates for observing these nonlinear effects because they carry a large Berry curvature concentrated in small regions, i.e., near the Weyl points. We have implemented the semiclassical Berry curvature dipole formalism into an *ab initio* scheme and investigated the second-order nonlinear response for two representative groups of materials: the TaAs-family type-I WSMs and the MoTe₂-family type-II WSMs. Both types of WSMs exhibited a Berry curvature dipole in which type-II Weyl points are usually superior to the type-I WSM because of the strong tilt. Corresponding nonlinear susceptibilities in several materials promise a nonlinear Hall effect in the dc field limit, which is within the experimentally detectable range.

DOI: 10.1103/PhysRevB.97.041101

Introduction. The Weyl semimetal (WSM) [1–6] is a topological state characterized by linear band crossing points called Weyl points near the Fermi energy. WSM materials, such as the TaAs-family pnictides [7,8] and MoTe₂ [9,10], have recently been discovered primarily by observation of the unique Fermi arcs of surface states through angle-resolved photoemission spectroscopy [11–16]. Because Weyl points are monopole sources or drains of the Berry curvature of Bloch wave functions in momentum space, a WSM can exhibit an anomalous Hall effect when breaking the time-reversal symmetry (TRS) [17–19] or a spin Hall effect [20] as a linear response to an external electric field. Recent theoretical [21–31] and experimental [32–35] studies have revealed giant nonlinear optical responses in inversion-symmetry-breaking WSMs, such as the photocurrent from the circular photogalvanic effect (CPGE), second-harmonic generation (SHG), and the nonlinear Hall effect. These nonlinear effects can be much stronger in WSMs than traditional electro-optic materials owing to the large Berry curvature [22,36,37].

Very recently, the semiclassical approach has been used to describe the intraband contributions to CPGE and SHG as a Berry phase effect [36,37] by a geometric quantity: the Berry curvature dipole (BCD) [22]. At the dc limit, the photocurrent remains finite as a transverse Hall-like current, i.e., a nonlinear Hall effect [22]. These nonlinear effects originate from the intraband resonant transitions at a low frequency in a noncentrosymmetric metal. Although they have played an important role in predicting topological materials and estimating their linear-response properties, there is still a lack of *ab initio* studies on the nonlinear optical effects of WSMs to quantitatively reveal the role of the Weyl points in realistic materials [32]. The nonlinear response usually is computed with mixed interband and intraband transitions

for conventional semiconductors via the Berry connection related formalism [38,39], but an *ab initio* scheme with the Berry curvature dipole would be required to understand the contribution from Weyl fermions.

We studied the BCD of WSM materials, i.e., TaAs-family type-I and MoTe₂-family type-II WSMs and estimated their nonlinear optical responses by *ab initio* calculations combined with the semiclassical approach. Both types of WSMs exhibit a large BCD near the Weyl point that is orders of magnitude larger than that of conventional materials. As a Fermi surface property, the BCD favors tilted Weyl cones. Thus, the type-II WSM is usually superior to the type-I WSM. Furthermore, we found that some small gap regions with highly concentrated Berry curvature also can contribute to a large dipole in the absence of Weyl points, similar as the enhancement of the bulk photovoltaic effect in topological insulators [40]. We made an order-of-magnitude estimate of the nonlinear Hall effect for these materials, which is experimentally accessible.

Semiclassical theory. We first overview previous theoretical work on the nonlinear optical response described by the Berry curvature [22,25,36,37]. For the CPGE, the oscillating electric field $E_c(t) = \text{Re}\{\mathcal{E}_c e^{i\omega t}\}$ of circularly polarized light induces a dc photocurrent $\mathbf{j}^{(0)}$ as a second-order nonlinear optical effect: $\mathbf{j}_a^{(0)} = \chi_{abc} \mathcal{E}_b \mathcal{E}_c^*$. Similarly, the SHG is described by the second-harmonic current response $\mathbf{j}^{(2\omega)} e^{2i\omega t}$ to a linearly polarized light, where $\mathbf{j}_a^{(2\omega)} = \chi_{abc} \mathcal{E}_b \mathcal{E}_c$. At the dc limit of a linearly polarized field, the nonlinear Hall effect is characterized by a transverse current: $j_a = 2j_a^{(0)}|_{\omega \rightarrow 0} = 2\chi_{abb}|\mathcal{E}_b|^2$. For a material with TRS, the nonlinear-response tensor σ has been obtained theoretically as a Berry phase effect [36,37] and very recently further described by the BCD [22] as follows:

$$\chi_{abc} = -\varepsilon_{adc} \frac{e^3 \tau}{2\hbar^2(1 + i\omega\tau)} D_{bd}, \quad (1)$$

$$D_{bd} = \int_k f_0 \frac{\partial \Omega_d}{\partial k_b}, \quad (2)$$

*binghai.yan@weizmann.ac.il

where D_{bd} is the BCD, Ω_d is the Berry curvature, f_0 is the equilibrium Fermi-Dirac distribution, τ refers to the relaxation time approximation in the Boltzmann equation, ε_{adc} stands for the third-rank Levi-Civita symbol, and \hbar is the reduced Planck constant. D_{bd} is a Fermi-surface effect that is intrinsic to the band structure and becomes dimensionless in three dimensions. We define the BCD density in the k space as $d_{bd} \equiv f_0 \frac{\partial \Omega_d}{\partial k_b}$. Because d_{bd} is odd to the space inversion, D_{bd} vanishes when inversion symmetry appears. Although they were obtained with the semiclassical theory, Eqs. (1) and (2) can also be derived by a fully quantum theoretical treatment with the Floquet formalism [25].

Ab initio calculation methods. We performed *ab initio* density-functional theory (DFT) calculations for the bulk materials and projected Bloch wave functions to atomiclike local Wannier functions with the full-potential local-orbital (FPLO) program [41] within the generalized gradient approximation [42]. For a material, we obtained the tight-binding Hamiltonian \hat{H} . Note that \hat{H} inherits exactly all symmetries of the system, which is crucial for accurate evaluation of the BCD from the Berry curvature Ω in a differential manner [43]. The Berry curvature [44] of the n th band can be calculated according to \hat{H} ,

$$\Omega_a^n(\mathbf{k}) = \varepsilon_{abc} 2i \sum_{m \neq n} \frac{\langle n | \partial_{k_b} \hat{H} | m \rangle \langle m | \partial_{k_c} \hat{H} | n \rangle}{(\epsilon_n - \epsilon_m)^2}, \quad (3)$$

where ϵ_n and $|n\rangle$ are eigenvalues and eigenwave functions, respectively, of \hat{H} at the momentum \mathbf{k} . Ω_a^n runs over occupied bands in Eq. (2), where $\Omega_d = \sum_n \Omega_d^n$.

Simple effective model of Weyl points. Before visiting specific WSM materials, we investigated the BCD for a simple Weyl Hamiltonian to reach a qualitative but inspiring understanding,

$$H_{\text{Weyl}}(\mathbf{q}) = \hbar v_t q_t \sigma_0 + \hbar v_F \mathbf{q} \cdot \boldsymbol{\sigma}, \quad (4)$$

where \mathbf{q} is the momentum with respect to the Weyl point, $\boldsymbol{\sigma}$ is the Pauli matrix vector, v_F is the Fermi velocity of an isotropic Weyl cone without tilt, v_t represents the tilting velocity, and q_t is the tilting momentum along the \hat{t} direction. The tilt of the Weyl cone is characterized by the ratio $|v_t/v_F|$, where $|v_t/v_F| < 1$ stands for a type-I Weyl cone and $|v_t/v_F| > 1$ stands for a type-II one. Because the Berry curvature is $\Omega(\mathbf{q}) = \frac{\mathbf{q}}{2q^3}$ for the lower cone, we analytically can obtain d_{xy} , for example, without loss of generality,

$$d_{xy} = \frac{\partial \Omega_y}{\partial q_x} = \frac{3q_x q_y}{2q^5}. \quad (5)$$

We note that Ω and d_{xy} are independent of the tilt and reverse sign for the upper cone. However, the shape of the Fermi surface is sensitive to the tilt.

The d_{xy} exhibits xy -type symmetry near the Weyl point [Eq. (5)], which resembles a “ d_{xy} -type” atomic wave function in real space. For a type-I WSM, D_{xy} diminishes when E_F crosses the Weyl point because the integral of d_{xy} leads to zero owing to the xy -type symmetry. This is fully consistent with the fact that D_{xy} vanishes as the Fermi surface shrinks to a point at the Weyl point. When E_F lies either below or above the Weyl point, the Fermi-surface region effectively is subtracted from the sum over the lower cone. If the type-I Weyl cone

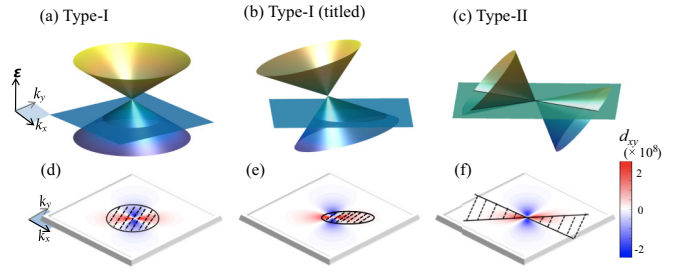


FIG. 1. The Weyl cones and the dipole moment distribution of the Berry curvature. (a) A standard type-I Weyl cone without tilting. The Fermi energy is indicated by the horizontal plane, and the Fermi surface is a circle. Corresponding dipole moment of the Berry curvature is shown in (d) near the Weyl point. (b) A type-I Weyl cone with a slight tilting and corresponding dipole moment in (e). (c) A type-II Weyl cone with a strong tilting and corresponding dipole moment in (f). Near the Weyl point, the dipole moment exhibits a symmetric $k_x k_y$ -type distribution when the Fermi energy crosses a type-I Weyl point, and thus, it is summed to be zero as integrating over the k space. In (d) and (e), the circle with a shadow region indicates the unoccupied bands that do not contribute to the integral of the dipole moment. The blue and red colors show negative and positive values of the dipole moment. In (f), the shadowed regions stand for the unoccupied hole pocket and the occupied electron band, both of which are deducted from the integral of the dipole moment.

has no tilt [see Fig. 1(a)], the Fermi surface is centered on the Weyl point. Thus, d_{xy} outside the Fermi-surface region is still highly symmetric and summed up to be zero. If the type-I Weyl cone has a tilt along some arbitrary direction [see Fig. 1(b)], the Fermi-surface center is shifted away from the Weyl point. Consequently, d_{xy} outside the Fermi-surface region becomes asymmetric, which leads to a nonzero net D_{xy} . For a type-II Weyl cone [see Fig. 1(c)], the Fermi surface naturally breaks the xy -type symmetries of d_{xy} and thus presents a nonzero D_{xy} . We simply can summarize these optimal conditions for a large D_{xy} near a single Weyl point: (i) For a type-I Weyl point, a tilt is necessary, which is common for WSM materials. Because d_{xy} is highly concentrated near the Weyl point, E_F should stay close enough to the Weyl point. (ii) The type-II Weyl point may exhibit large D_{xy} , even when E_F crosses it. Although the large tilt of the Weyl points also was predicted to generate photocurrents by Chan *et al.* [29], they referred to the resonant transition between occupied and empty bands of the Weyl cone, which is different from the current finding in the low-frequency intraband transition.

Furthermore, we point out that a pair of Weyl points that are the \mathcal{M}_x , \mathcal{M}_y , or TRS partners contribute the same D_{xy} because $d_{xy} = d\Omega_y/dq_x$ is even for \mathcal{M}_x , \mathcal{M}_y , or TRS. Therefore, multiple Weyl points related to TRS and mirror symmetries multiply their contributions to the BCD instead of compensating for each other.

Realistic materials. We investigated two representative families of materials with inversion-symmetry breaking: (Ta, Nb)(As, P) as type-I WSMs and (Mo, W)Te₂ as type-II WSMs. For a given material, the BCD tensor D_{ab} shape can be analyzed by considering the corresponding point-group symmetry [22]. For instance, TaAs-type compounds belong to the C_{4v} point group, where \mathcal{M}_x and \mathcal{M}_y reflection symmetries exist.

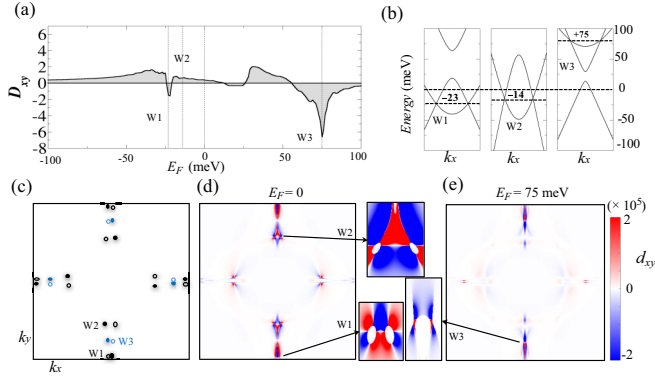


FIG. 2. Calculated Berry curvature dipole D_{xy} for TaAs. (a) The Fermi energy (E_F) dependence of D_{xy} . $E_F = 0$ corresponds to the charge neutral point. (b) The band dispersions crossing a pair of Weyl points. Three types of Weyl points, W1, W2, and W3, are shown. (c) The projection of three types of Weyl points on the $k_x k_y$ plane by integrating d_{xy} over k_z . The distribution of d_{xy} at (d) $E_F = 0$ and (e) $E_F = 75$ meV crossing W3. Red and blue represent the positive and negative values of d_{xy} , respectively, in arbitrary units. In the insets, d_{xy} distributions near some Weyl points are shown on the $k_x k_y$ plane without integrating the k_z direction. The full Brillouin zone projected on the $k_x k_y$ plane is shown here.

Because Ω_x and k_x are even and odd, respectively, for \mathcal{M}_x , d_{xx} is odd for \mathcal{M}_x , so $D_{xx} = 0$. Similarly, $D_{yy} = D_{zz} = 0$. Because Ω_z and k_x are odd and even, respectively, for \mathcal{M}_y , d_{xz} is odd for \mathcal{M}_y , so $D_{xz} = 0$. Likewise, we obtain only two nonzero tensor elements D_{xy} and D_{yx} , which follow $D_{xy} = -D_{yx}$. For (Mo,W)Te₂ in the C_{2v} point group, we obtain two non-zero-independent tensor elements: D_{xy} and D_{yx} .

Because it is a Fermi-surface property, the BCD relies on the Fermi energy in the band structure. As shown in Figs. 2(a) and 2(b), D_{xy} of TaAs exhibits a sensitive dependence on the Fermi energy. Two groups of type-I Weyl points are known to exist owing to the crossings between the top valence and the bottom conduction bands: four pairs of Weyl points, noted as W1 on the $k_z = 0$ plane; and eight pairs of Weyl points, noted as W2 on the $k_z \approx \pi/c$ plane (c is the lattice parameter along the z axis). W1 and W2 lie 23 and 14 meV, respectively, below the charge neutral point ($E_F = 0$) [see Fig. 2(b)]. This is consistent with previous calculations and experimental measurements [45]. D_{xy} shows a peak in magnitude when E_F is close to W1, whereas it reverses the sign without a clear peak when E_F approaches W2. Although D_{xy} is zero as E_F exactly meets the Weyl point, the induced small D_{xy} region can be very narrow compared to the energy sampling interval [0.1 meV in Fig. 2(a)]. Thus, D_{xy} does not necessarily show an apparent dip in amplitude at W1 or W2. Because $E_F = 0$ is slightly away from the Weyl points, D_{xy} here is weaker in magnitude than those near W1 or W2. Figure 2(d) plots d_{xy} projected on the $k_x k_y$ plane. It is clear that d_{xy} is distributed mainly in the W1 and W2 regions near the \mathcal{M}_x plane but not the \mathcal{M}_y mirror plane. The small gap regions near the Weyl points also contribute stronger magnitudes for $|d_{xy}|$. Note that d_{xy} does not necessarily follow the C_4 rotational symmetry. When the vicinity of W1 or W2 is magnified, a roughly xy -like distribution and an ellipselike hollow region

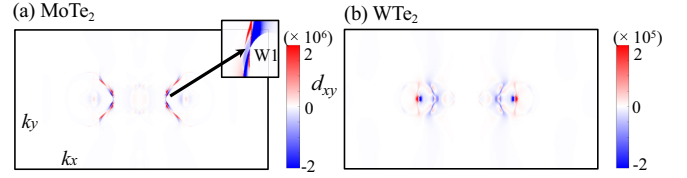


FIG. 3. Berry curvature dipole for (a) MoTe₂ and (b) WTe₂ projected on the $k_x k_y$ plane for $E_F = 0$. The first Brillouin zone is shown on the $k_x k_y$ plane. A Weyl point region is magnified to demonstrate the type-II Weyl point feature. We point out that the scale of the color bar in (a) is one order of magnitude larger than that in (b).

can be observed. Such a hollow region corresponds to the Fermi surface that surrounds a Weyl point. This is similar to the effective deduction of the Fermi surface of a tilted Weyl cone as demonstrated in Fig. 1(b). Another striking feature is the large peak of D_{xy} at $E_F = 75$ meV. At this energy, we actually observed eight pairs of new Weyl points (noted as W3) by the crossings between the lowest and the second-lowest conduction bands [see Fig. 2(b)]. The W3 Weyl points are located between W1 and W2 in the momentum space and belong to type II as revealed by their energy dispersions. The corresponding d_{xy} indeed presents hot spots near W3, similar to that shown in Fig. 1(c). This further confirms that type-II Weyl points contribute a larger BCD than type-I Weyl points under similar material conditions.

We now turn to the type-II WSMs: MoTe₂ and WTe₂. In band structures, we obtained two pairs of type-II Weyl points for MoTe₂ and no Weyl point for WTe₂ between their conduction and valence bands, which is slightly different from the literature [9,10]. This discrepancy is caused by the subtle difference between different DFT methods as revealed in recent calculations [46,47]. Here, WTe₂ serves as an example of a non-WSM for the purpose of comparison to a WSM. For MoTe₂, we labeled the Weyl points as W1. For W1 points located nearly at $E_F = 0$, D_{xy} indeed shows a peak here. Near W1, the profile of d_{xy} looks like two crossing lines, which is a typical feature of the type-II Weyl point [see Fig. 3(a)]. In contrast, WTe₂ exhibits a much smaller D_{xy} than MoTe₂. Although some hot spots of d_{xy} appear in Fig. 3(b), they are less focused and one order of magnitude smaller than those of MoTe₂.

Discussion. Based on the results for TaAs, MoTe₂, and WTe₂, we verified these features of BCD as observed in simple models. Weyl points induce a large BCD, and type-II Weyl

TABLE I. The Berry curvature dipole calculated for Weyl semimetal materials. The Fermi energy is set to the charge neutral point. Only the nonzero tensor elements are listed for a given material, which are dimensionless.

Material	D_{xy}	Material	D_{xy}	D_{yx}
TaAs	0.39	MoTe ₂	0.849	-0.703
TaP	0.029	WTe ₂	0.048	-0.066
NbAs	-9.88			
NbP	20.06			

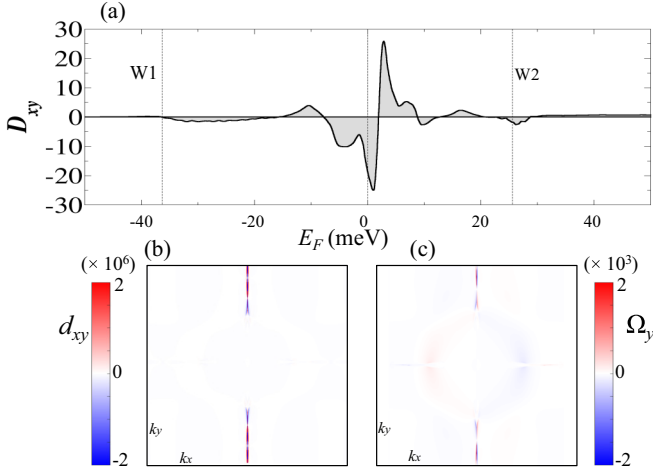


FIG. 4. Berry curvature dipole for NbP for $E_F = 0$. (a) The energy-dependent D_{xy} . W1 and W2 Weyl points lie below and above, respectively, the charge neutral point as indicated. (b) The d_{xy} and (c) Ω_y distributions at $E_F = 0$. Both are shown in arbitrary units.

points usually contribute much more than type-I Weyl points. A WSM possibly exhibits a much stronger nonlinear response than an ordinary metal.

Furthermore, we reveal some new features of a BCD when all six compounds in Table I are compared. It is known that TaAs, TaP, NbAs, and NbP exhibit a decreasing order of spin-orbit coupling (SOC), which leads to a similarly decreasing order of the spin Hall effect [20]. However, D_{xy} does not follow the same order of SOC. NbAs and NbP show a much larger D_{xy} than other materials, including MoTe₂.

Take NbP as an example. Its W1 Weyl points (36 meV below $E_F = 0$) present rather small D_{xy} 's because they are type I with a weak tilt. In contrast, its W2 points (26 meV above $E_F = 0$) contribute a peak of D_{xy} as shown in Fig. 4(a) because they are type II as revealed recently [48]. Although W1 and W2 still fit the above understanding about Weyl points, there are two large peaks of D_{xy} near $E_F = 0$ where only trivial Fermi pockets exist [49], which implies unusual D_{xy} contributions beyond the Weyl points. We found that d_{xy} is distributed dominantly along the \mathcal{M}_x mirror plane [Fig. 4(b)]. This can be rationalized by the distribution of the Berry curvature Ω_y . Ω_y is odd for \mathcal{M}_x and even for \mathcal{M}_y . Therefore, the Ω_y gradient along k_x , i.e., $d_{xy} = \partial\Omega_y/\partial k_x$, is large when crossing the \mathcal{M}_x plane. Furthermore, Ω_y is more concentrated in a small region very close to the \mathcal{M}_x plane in NbP than in TaAs, which further enhances d_{xy} in NbP. Such a difference between NbP and TaAs originates from their band structures of SOC. At the limit of zero SOC,

the valence and conduction bands each cross inside a mirror plane, which gives rise to a mirror symmetry protected nodal ring for the two systems. As the SOC increases, the nodal ring is gapped out. Consequently, the Berry curvature that is caused by the entanglement between the valence and the conduction bands has a more extended distribution in momentum space as indicated by Eq. (3). Therefore, TaAs with a stronger SOC exhibits a much smaller BCD than NbP.

The sensitive Fermi-surface dependence of the BCD serves as a way to effectively tune the nonlinear response in WSM materials. For example, both the carrier doping and the external pressure are known to engineer the Fermi surface of these compounds (e.g., Refs. [10,46,50–52]). To enhance the BCD, it is favored that the material exhibits Weyl points and/or small energy gaps at the Fermi energy. The material with nodal lines in the absence of SOC may lead to Weyl points and small gap regions near these nodal lines when weak SOC is turned on without the inversion symmetry, presenting a large volume of BCD distribution near nodal lines (e.g., NbP). Such nodal lines usually required the protection of mirror planes in the material structure.

Finally, we developed a semiquantitative estimation of the nonlinear response for these materials. According to Eq. (3), D_{xy} corresponds to χ_{zxx} and χ_{xxz} , and D_{yx} corresponds to χ_{zyy} and χ_{yyz} . We considered the nonlinear Hall effect where the transverse Hall-like current is $j_z = 2\chi_{zxx}\mathcal{E}_x^2$. The longitudinal current is $j_x = \sigma_{xx}\mathcal{E}_x$, and σ_{xx} is the ordinary conductivity. To characterize the strength of the nonlinear Hall effect, we can define the Hall angle as $\gamma = j_z/j_x = 2(\chi_{zxx}/\sigma_{xx})\mathcal{E}_x$. It is known that $\gamma \sim 10^{-3}$ for materials with the usual anomalous Hall effect (see Ref. [53] for a review). We assumed the relaxation time $\tau \sim 10$ ps and $\sigma_{xx} \sim 10^6 \Omega^{-1} \text{m}^{-1}$ based on recent low-temperature experiments (e.g., Refs. [54–58]) and an electric-field $\mathcal{E}_x \sim 10^2$ V/m that is applicable for a physical property measurement system in a laboratory. Then, we obtained $\chi_{zxx} \sim 10^{-1} D_{xy}$ and $\gamma \sim 10^{-5} - 10^{-4}$ for D_{xy} in the range of TaAs, MoTe₂, NbAs, and NbP. Because γ of the nonlinear Hall effect approaches 10% of that of anomalous Hall systems, the nonlinear Hall effect can be measurable for these WSM compounds.

Acknowledgments. We thank Professor C. Felser, Professor J. van den Brink, Professor C. Kane, Professor E. Mele, and Dr. I. Sodemann for helpful discussions. Y.Z. acknowledges financial support from the German Research Foundation (DFG, Grant No. SFB 1143). B.Y. was supported by a research grant from the Benozio Endowment Fund for the Advancement of Science and by a Grant from the German-Israeli Foundation for Scientific Research and Development (GIF Grant No. I-1364-303.7/2016).

[1] X. G. Wan, A. M. Turner, A. Vishwanath, and S. Y. Savrasov, *Phys. Rev. B* **83**, 205101 (2011).
[2] G. E. Volovik, *The Universe in A Helium Droplet* (Clarendon Press, Oxford, 2003).
[3] A. A. Burkov, M. D. Hook, and L. Balents, *Phys. Rev. B* **84**, 235126 (2011).
[4] P. Hosur and X. L. Qi, *C. R. Phys.* **14**, 857 (2013).
[5] B. Yan and C. Felser, *Annu. Rev. Condens. Matter Phys.* **8**, 337 (2017).

[6] N. P. Armitage, E. J. Mele, and A. Vishwanath [Rev. Mod. Phys. (to be published)], [arXiv:1705.01111](https://arxiv.org/abs/1705.01111).
[7] H. Weng, C. Fang, Z. Fang, B. A. Bernevig, and X. Dai, *Phys. Rev. X* **5**, 011029 (2015).
[8] S.-M. Huang, S.-Y. Xu, I. Belopolski, C.-C. Lee, G. Chang, B. Wang, N. Alidoust, G. Bian, M. Neupane, C. Zhang, S. Jia, A. Bansil, H. Lin, and M. Z. Hasan, *Nat. Commun.* **6**, 8373 (2015).
[9] A. A. Soluyanov, D. Gresch, Z. Wang, Q. Wu, M. Troyer, X. Dai, and B. A. Bernevig, *Nature (London)* **527**, 495 (2015).

- [10] Y. Sun, S. C. Wu, M. N. Ali, C. Felser, and B. Yan, *Phys. Rev. B* **92**, 161107(R) (2015).
- [11] B. Q. Lv, H. M. Weng, B. B. Fu, X. P. Wang, H. Miao, J. Ma, P. Richard, X. C. Huang, L. X. Zhao, G. F. Chen, Z. Fang, X. Dai, T. Qian, and H. Ding, *Phys. Rev. X* **5**, 031013 (2015).
- [12] S.-Y. Xu, I. Belopolski, N. Alidoust, M. Neupane, G. Bian, C. Zhang, R. Sankar, G. Chang, Y. Zhujun, C.-C. Lee, H. Shin-Ming, H. Zheng, J. Ma, D. S. Sanchez, B. Wang, A. Bansil, F. Chou, P. P. Shibayev, H. Lin, S. Jia, and M. Z. Hasan, *Science* **349**, 613 (2015).
- [13] L. X. Yang, Z. K. Liu, Y. Sun, H. Peng, H. F. Yang, T. Zhang, B. Zhou, Y. Zhang, Y. F. Guo, M. Rahn, D. Prabhakaran, Z. Hussain, S. K. Mo, C. Felser, B. Yan, and Y. L. Chen, *Nat. Phys.* **11**, 728 (2015).
- [14] K. Deng, G. Wan, P. Deng, K. Zhang, S. Ding, E. Wang, M. Yan, H. Huang, H. Zhang, Z. Xu, J. Denlinger, A. Fedorov, H. Yang, W. Duan, H. Yao, Y. Wu, S. Fan, H. Zhang, X. Chen, and S. Zhou, *Nat. Phys.* **12**, 1105 (2016).
- [15] J. Jiang, Z. K. Liu, Y. Sun, H. F. Yang, C. R. Rajamathi, Y. P. Qi, L. X. Yang, C. Chen, H. Peng, C. C. Hwang, S. Z. Sun, S.-K. Mo, I. Vobornik, J. Fujii, S. Parkin, C. Felser, B. Yan, and Y. L. Chen, *Nat. Commun.* **8**, 13973 (2017).
- [16] L. Huang, T. M. McCormick, M. Ochi, Z. Zhao, M.-T. Suzuki, R. Arita, Y. Wu, D. Mou, H. Cao, J. Yan, N. Trivedi, and A. Kaminski, *Nat. Mater.* **15**, 1155 (2016).
- [17] G. Xu, H. Weng, Z. Wang, X. Dai, and Z. Fang, *Phys. Rev. Lett.* **107**, 186806 (2011).
- [18] K.-Y. Yang, Y.-M. Lu, and Y. Ran, *Phys. Rev. B* **84**, 075129 (2011).
- [19] A. A. Burkov, *Phys. Rev. Lett.* **113**, 187202 (2014).
- [20] Y. Sun, Y. Zhang, C. Felser, and B. Yan, *Phys. Rev. Lett.* **117**, 146403 (2016).
- [21] P. Hosur and X.-L. Qi, *Phys. Rev. B* **91**, 081106 (2015).
- [22] I. Sodemann and L. Fu, *Phys. Rev. Lett.* **115**, 216806 (2015).
- [23] T. Morimoto and N. Nagaosa, *Sci. Adv.* **2**, e1501524 (2016).
- [24] K. Taguchi, T. Imaeda, M. Sato, and Y. Tanaka, *Phys. Rev. B* **93**, 201202 (2016).
- [25] T. Morimoto, S. Zhong, J. Orenstein, and J. E. Moore, *Phys. Rev. B* **94**, 245121 (2016).
- [26] C.-K. Chan, P. A. Lee, K. S. Burch, J. H. Han, and Y. Ran, *Phys. Rev. Lett.* **116**, 026805 (2016).
- [27] H. Ishizuka, T. Hayata, M. Ueda, and N. Nagaosa, *Phys. Rev. Lett.* **117**, 216601 (2016).
- [28] F. de Juan, A. G. Grushin, T. Morimoto, and J. E. Moore, *Nat. Commun.* **8**, 15995 (2017).
- [29] C.-K. Chan, N. H. Lindner, G. Refael, and P. A. Lee, *Phys. Rev. B* **95**, 041104 (2017).
- [30] H. Rostami and M. Polini, *arXiv:1705.09915*.
- [31] E. J. König, H.-Y. Xie, D. A. Pesin, and A. Levchenko, *Phys. Rev. B* **96**, 075123 (2017).
- [32] L. Wu, S. Patankar, T. Morimoto, N. L. Nair, E. Thewalt, A. Little, J. G. Analytis, J. E. Moore, and J. Orenstein, *Nat. Phys.* **13**, 350 (2017).
- [33] Q. Ma, S.-Y. Xu, C.-K. Chan, C.-L. Zhang, G. Chang, Y. Lin, W. Xie, T. Palacios, H. Lin, S. Jia, P. A. Lee, P. Jarillo-Herrero, and N. Gedik, *Nat. Phys.* **13**, 842 (2017).
- [34] K. Sun, S. Sun, C. Guo, L. Wei, H. Tian, H. Yang, G. Chen, and J. Li, *Chin. Phys. Lett.* **34**, 117203 (2017).
- [35] S. Chi, Z. Li, Y. Xie, Y. Zhao, Z. Wang, L. Li, H. Yu, G. Wang, H. Weng, H. Zhang, and J. Wang, *arXiv:1705.05086*.
- [36] J. E. Moore and J. Orenstein, *Phys. Rev. Lett.* **105**, 026805 (2010).
- [37] E. Deyo, L. E. Golub, E. L. Ivchenko, and B. Spivak, *arXiv:0904.1917*.
- [38] J. E. Sipe and A. I. Shkrebtii, *Phys. Rev. B* **61**, 5337 (2000).
- [39] S. M. Young and A. M. Rappe, *Phys. Rev. Lett.* **109**, 116601 (2012).
- [40] L. Z. Tan and A. M. Rappe, *Phys. Rev. Lett.* **116**, 237402 (2016).
- [41] K. Koepf and H. Eschrig, *Phys. Rev. B* **59**, 1743 (1999).
- [42] J. P. Perdew, K. Burke, and M. Ernzerhof, *Phys. Rev. Lett.* **77**, 3865 (1996).
- [43] For the integrals of D_{xy} , the first Brillouin zone was sampled by k grids from $200 \times 200 \times 200$ to $1000 \times 1000 \times 1000$. Satisfactory convergence was achieved for a k grid of $800 \times 800 \times 800$ for all compounds. Increasing the grid size to $1000 \times 1000 \times 1000$ only varies the D_{xy} value by no more than 5%.
- [44] D. Xiao, M.-C. Chang, and Q. Niu, *Rev. Mod. Phys.* **82**, 1959 (2010).
- [45] F. Arnold, M. Naumann, S. C. Wu, Y. Sun, M. Schmidt, H. Borrmann, C. Felser, B. Yan, and E. Hassinger, *Phys. Rev. Lett.* **117**, 146401 (2016).
- [46] Z. Wang, D. Gresch, A. A. Soluyanov, W. Xie, S. Kushwaha, X. Dai, M. Troyer, R. J. Cava, and B. A. Bernevig, *Phys. Rev. Lett.* **117**, 056805 (2016).
- [47] F. Y. Bruno, A. Tamai, Q. S. Wu, I. Cucchi, C. Barreteau, A. de la Torre, S. McKeown Walker, S. Riccò, Z. Wang, T. K. Kim, M. Hoesch, M. Shi, N. C. Plumb, E. Giannini, A. A. Soluyanov, and F. Baumberger, *Phys. Rev. B* **94**, 121112(R) (2016).
- [48] S.-C. Wu, Y. Sun, F. Claudia, and B. Yan, *Phys. Rev. B* **96**, 165113 (2017).
- [49] J. Klotz, S.-C. Wu, C. Shekhar, Y. Sun, M. Schmidt, M. Nicklas, M. Baenitz, M. Uhlarz, J. Wosnitza, C. Felser, and B. Yan, *Phys. Rev. B* **93**, 121105 (2016).
- [50] R. D. dos Reis, S. C. Wu, Y. Sun, M. O. Ajeesh, C. Shekhar, M. Schmidt, C. Felser, B. Yan, and M. Nicklas, *Phys. Rev. B* **93**, 205102 (2016).
- [51] I. Belopolski, D. S. Sanchez, Y. Ishida, X. Pan, P. Yu, S.-Y. Xu, G. Chang, T.-R. Chang, H. Zheng, N. Alidoust, G. Bian, M. Neupane, S.-M. Huang, C.-C. Lee, Y. Song, H. Bu, G. Wang, S. Li, G. Eda, H.-T. Jeng, T. Kondo, H. Lin, Z. Liu, F. Song, S. Shin, and M. Z. Hasan, *Nat. Commun.* **7**, 13643 (2016).
- [52] M. Einaga, K. Shimizu, J. Hu, Z. Q. Mao, and A. Politano, *Phys. Status Solidi RRL* **11**, 1700182 (2017).
- [53] N. Nagaosa, J. Sinova, S. Onoda, A. H. MacDonald, and N. P. Ong, *Rev. Mod. Phys.* **82**, 1539 (2010).
- [54] C. Shekhar, A. K. Nayak, Y. Sun, M. Schmidt, M. Nicklas, I. Leermakers, U. Zeitler, Y. Skourski, J. Wosnitza, Z. Liu, Y. Chen, W. Schnelle, H. Borrmann, Y. Grin, C. Felser, and B. Yan, *Nat. Phys.* **11**, 645 (2015).
- [55] F. Arnold, C. Shekhar, S.-C. Wu, Y. Sun, R. D. dos Reis, N. Kumar, M. Naumann, M. O. Ajeesh, M. Schmidt, A. G. Grushin, J. H. Bardarson, M. Baenitz, D. Sokolov, H. Borrmann,

- M. Nicklas, C. Felser, E. Hassinger, and B. Yan, [Nat. Commun.](#) **7**, 11615 (2016).
- [56] C.-L. Zhang, S.-Y. Xu, I. Belopolski, Z. Yuan, Z. Lin, B. Tong, G. Bian, N. Alidoust, C.-C. Lee, S.-M. Huang, T.-R. Chang, G. Chang, C.-H. Hsu, H.-T. Jeng, M. Neupane, D. S. Sanchez, H. Zheng, J. Wang, H. Lin, C. Zhang, H.-Z. Lu, S.-Q. Shen, T. Neupert, M. Zahid Hasan, and S. Jia, [Nat. Commun.](#) **7**, 10735 (2016).
- [57] X. Huang, L. Zhao, Y. Long, P. Wang, D. Chen, Z. Yang, H. Liang, M. Xue, H. Weng, Z. Fang, X. Dai, and G. Chen, [Phys. Rev. X](#) **5**, 031023 (2015).
- [58] Y. Qi, P. G. Naumov, M. N. Ali, C. R. Rajamathi, W. Schnelle, O. Barkalov, M. Hanfland, S.-C. Wu, C. Shekhar, Y. Sun, V. Suß, M. Schmidt, U. Schwarz, E. Pippel, P. Werner, R. Hillebrand, T. Forster, E. Kampert, S. Parkin, R. J. Cava, C. Felser, B. Yan, and S. A. Medvedev, [Nat. Commun.](#) **7**, 11038 (2016).